Electric field measurements in a kHz-driven He jet - The influence of the gas flow speed

Electric field measurements in a kHz-driven He jet—the influence of the gas flow speed

2016 Plasma Sources Sci. Technol. 25 065026

(http://iopscience.iop.org/0963-0252/25/6/065026)

IOP Publishing Plasma Sources Science and Technology

Plasma Sources Sci. Technol. **25** (2016) 065026 (9pp) doi:10.1088/0963-0252/25/6/065026

Electric field measurements in a kHz-driven He jet—the influence of the gas flow speed

A Sobota[1], O Guaitella[2], G B Sretenović[3], I B Krstić[3], V V Kovačević[3], A Obrusník[4], Y N Nguyen[1], L Zajíčková[4,5], B M Obradović[3] and M M Kuraica[3]

[1] Eindhoven University of Technology, EPG, Postbus 513, 5600MB Eindhoven, The Netherlands
[2] LPP, Ecole Polytechnique, Route de Saclay, 91128 Palaiseau, France
[3] University of Belgrade, Faculty of Physics, PO Box 44, 11001 Belgrade, Serbia
[4] Department of Physical Electronics at the Faculty of Science, Masaryk University, Kotlarska 2, 61137 Brno, Czech Republic
[5] Plasma Technologies at CEITEC, Masaryk University, Kotlarska 2, 61137 Brno, Czech Republic

E-mail: a.sobota@tue.nl

Received 12 April 2016, revised 22 September 2016
Accepted for publication 6 October 2016
Published 18 November 2016

Abstract

This report focuses on the dependence of electric field strength in the effluent of a vertically downwards-operated plasma jet freely expanding into room air as a function of the gas flow speed. A 30 kHz AC-driven He jet was used in a coaxial geometry, with an amplitude of 2 kV and gas flow between 700 sccm and 2000 SCCM. The electric field was measured by means of Stark polarization spectroscopy of the He line at 492.19 nm. While the minimum and the maximum measured electric fields remained unchanged, the effect of the gas flow speed is to cause stretching of the measured profile in space—the higher the flow, the longer and less steep the electric field profile. The portion of the effluent in which the electric field was measured showed an increase of electric field with increasing distance from the capillary, for which the probable cause is the contraction of the plasma bullet as it travels through space away from the capillary. There are strong indications that the stretching of the electric field profile with increase in the flow speed is caused by differences in gas mixing as a function of the gas flow speed. The simulated gas composition shows that the amount of air entrained into the gas flow behaves in a similar way to the observed behaviour of the electric field. In addition we have shown that the visible length of the plasma plume is associated with a 0.027 molar fraction of air in the He flow in this configuration, while the maximum electric field measured was associated with a 0.014 molar fraction of air at gas flow rates up to 1500 SCCM (4.9 m s^{-1}). At higher flows vortices occur in the effluent of the jet, as seen in Schlieren visualization of the gas flow with and without the discharge.

Keywords: discharge, plasma jet, atmospheric pressure, helium, ionization front, plasma bullet, electric field

(Some figures may appear in colour only in the online journal)

1. Introduction

Because of the simplicity of their construction and operation, as well as their potential in biomedical applications or other types of surface treatment [1–4], atmospheric pressure plasma jets have been extensively studied in the last 20 years. Even so, electric field measurements in this type of discharge are infrequent [5–11] because of the associated experimental difficulties.

Nonetheless, the magnitude of the electric field is of key importance for experimental and theoretical work on plasma jets, as well as their applications. It has been shown that

electric field can be a cause of various effects observed in experiments on biological samples [12–16]. In the field of plasma physics, in transient discharges with low ionization levels, such as plasma jets, the electric field is the driver of the discharge and its magnitude is the central component that determines its behavior and charge production [17], ultimately affecting the resulting chemistry.

Among the few published reports on electric fields in plasma jets operating at kHz frequencies, in the so-called 'bullet mode', there is no mention of the influence of flow speed on the discharge or the associated electric field. The role of the gas flow in the operation of the jet is still not clear. As a rule, the flow speed is orders of magnitude slower than the propagation of the ionization front either in the capillary or in the surrounding atmosphere [18–23]. In fact the body of gas flowing through the capillaries in jet systems typically moves less than 1 mm in an entire voltage cycle, while discharge development lasts only a fraction of that time [22]. Still, gas flow is indispensable for jet operation, even when the jet operates in flowing air [24].

This paper concerns measurements of electric field in the plume of an atmospheric pressure plasma jet operated in He using a 30 kHz sine voltage. The measurements were done in the freely expanding plume in room air, with the He flow directed downwards. The report shows the influence of the He flow speed on the axial electric field profile; the observed effects are analyzed through the gas composition profiles and associated ionization and attachment coefficients at different flows.

2. Experimental setup

The atmospheric pressure plasma jet used in this work has already been described in detail [22, 23]. A coaxial geometry is used, where the powered electrode is centered inside the Pyrex capillary (inner diameter 2.5 mm, outer diameter 4 mm) and a metal ring on the outer side of the capillary is used as the grounded electrode, as illustrated in the schematics on the left-hand side of figure 1. The thickness of the ground is 3 mm, and the gap between the two electrodes was 5 mm for the entire study.

The jet is powered by sine voltage at 30 kHz, 2 kV in amplitude (4 kV peak-to-peak). One ionization wave (guided streamer, plasma bullet) is formed and expelled into the room atmosphere in each voltage cycle in the positive half-period of the cycle, without the appearance of microdischarges, as reported in [22, 23].

The powered electrode also serves as a gas inlet (inner diameter 0.8 mm, outer diameter 1.6 mm). The discharge was formed using He flow (Messer, 99.996% purity). The jet was set up vertically, with the direction of the gas flow pointing downwards. Gas flow was regulated using a Bronkhorst® flow control system.

Electric field strength in a He plasma jet is measured using a method for electric field measurement developed by Kuraica and Konjević in the 1990s for a low-pressure glow discharge [25, 26], and later used for diagnostics of dielectric barrier discharges and plasma jets [5, 9, 27]. Essentially, this is a spectroscopic, non-perturbing method based on the Stark effect of He atoms. There are several electron transitions in the He atom that are forbidden by selection rules regarding orbital quantum number under unperturbed conditions, but the presence of an external electric field voids these restrictions, and generally forbidden lines start to appear in the spectrum. In addition, those lines shift as a function of the electric field strength. Forbidden lines are usually very close to the allowed lines, and it is most appropriate to calculate their positions as a function of the value of the external electric field using perturbation theory, as has been done in [25, 28, 29], and then use their mutual distance to determine of strength of the electric field. Depending on the change of the magnetic quantum number, emitted radiation is polarized parallel to the direction of the electric field (π-polarization) or normal to the direction of the electric field (σ-polarization, left or right). To measure the electric field, the polarizer is necessary to eliminate one of the polarized components—thus the method is called Stark polarization spectroscopy. In this paper we used the He (2^1P-4^1D) allowed line at 492.19 nm and the forbidden He (2^1P-4^1F) line nearest to it. The dependence of the electric field strength on the distance between these two lines is given by the following best fit formula [29]:

$$E(\mathrm{kV\ cm^{-1}}) = (-58.557 + 18.116\Delta\lambda_{\mathrm{FA}} + 3130.96\Delta\lambda_{\mathrm{FA}}^2 + 845.6\Delta\lambda_{\mathrm{FA}}^3)^{0.5} \quad (1)$$

where $\Delta\lambda_{\mathrm{FA}}$ is the shift of the centerline of the forbidden He (2^1P-4^1F) line from the allowed line at 492.19 nm. The experimental setup for the electrical and spectroscopic measurement is shown in the right-hand side of figure 1. The light emitted from the effluent of the plasma jet is focused on the slit of a 1 m Solar MSDD 1000 imaging spectrometer with a 1200 grooves $\mathrm{mm^{-1}}$ grating using an achromatic lens with a focal length of 150 mm. The object–image projection was 1:1, and the slit width was kept at 70 μm. A plastic polarizer is inserted between the lens and the slit in order to transmit only π-polarized light. The ICCD camera, Princeton Instruments PI-MAX2, is used to detect the dispersed light. The CCD has 1024×1024 pixels, and the full plasma jet length was imaged on the detector with 1:1 projection. The spatial resolution was 12.5 μm/pixel. The camera operated in gate mode and was synchronized with the current signal using the external trigger unit. The pixel-to-pixel resolution of the spectral apparatus was 0.0108 nm/pixel. The recordings were obtained with 90 accumulations and 100 000 exposures per accumulation.

The position of the peak of the forbidden He line was determined by a fitting procedure previously described in, for example, [5]. The peaks are fitted to better determine their position, as there is some overlap under the conditions of pressure broadening at 1 atm.

3. Results and analysis

3.1. Electric field in the plume as a function of gas flow speed

The electric field measurements as a function of the gas flow are shown on the left-hand side of figure 2. Several things

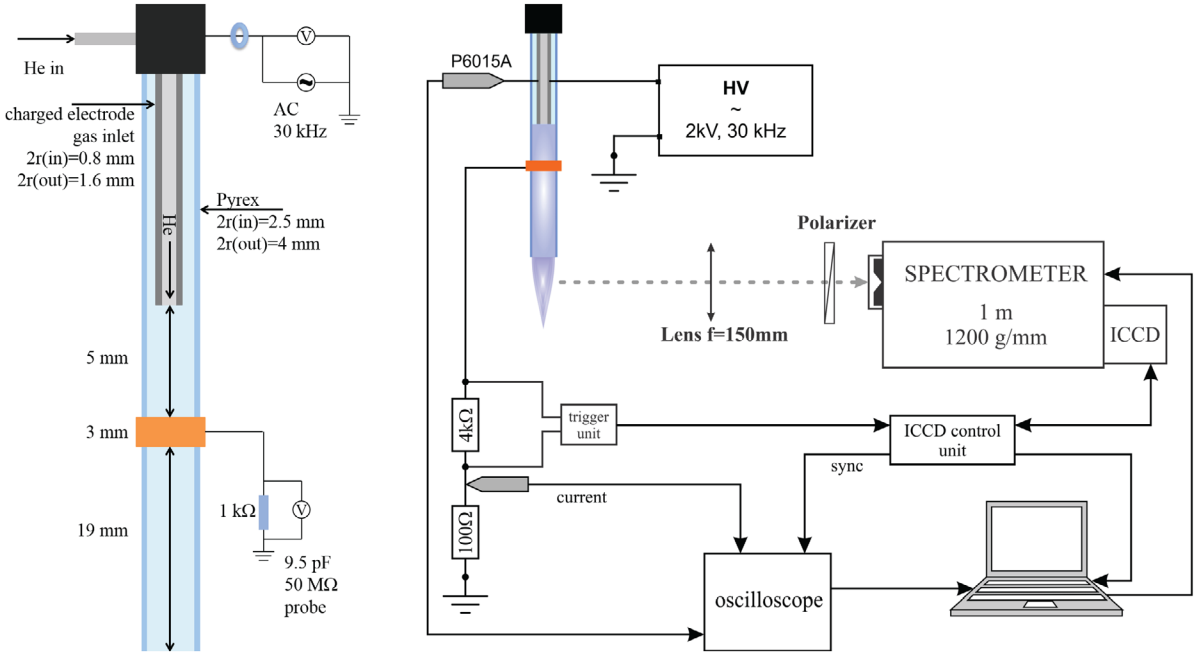

Figure 1. Schematics of the jet and the measurement setup [6, 9, 22]. Left: the downward vertically operated plasma jet is used in a coaxial configuration, where the inner charged electrode is also the gas inlet. The AC voltage at 30 kHz is applied with amplitude of 2 kV (4 kV peak-to-peak). Right: the optical emission spectroscopy setup consists of a monochromator and an intensified CCD (ICCD) camera, where the plume of the jet is imaged to the entrance slit of the monochromator in a 1:1 ratio.

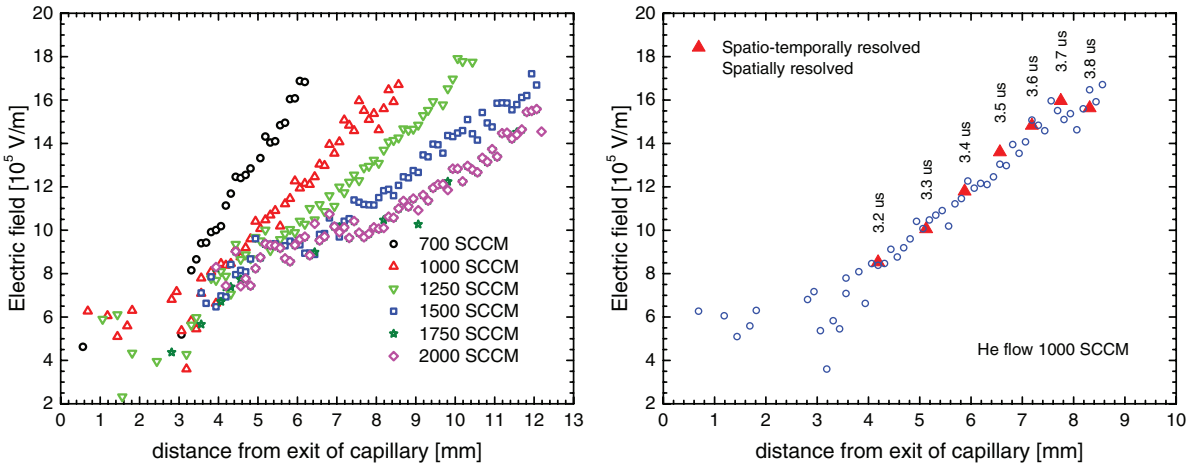

Figure 2. Electric field as a function of the gas flow speed in time-integrated measurements (left) and time-resolved measurements for one flow showing that the time-integrated measurements are representative of the evolution in space (right). The time indications on the right-hand graph represent the delay from the moment the plasma bullet is expelled under the grounded electrode, as described in [22].

can be noted on this graph: (i) although the measurements are time-integrated, their high spatial resolution allows the evolution of the electric field in time to be captured; (ii) the measured electric field increases with distance from the capillary; (iii) the He flow speed notably influences the distribution of the electric field. The following paragraphs analyze the results, bearing in mind each of these points.

3.1.1. Spatial and temporal resolution. When obtaining these data different exposure times (50 ns–3 μs) of the ICCD camera were used to temporally resolve the electric field in the plume of the jet. The graph on the right-hand side of figure 2 shows an overlay of two sets of measurements—one taken with an exposure time of 100 ns and one with an exposure time of 3 μs, when the time needed for the ionization wave to travel through the entire length of the plume is less than 3 μs.

The figure shows that the electric field data resulting from the time-resolved measurement (100 ns) is in excellent agreement with the data from the measurement that was not temporally resolved (3 μs). In the time-resolved measurement set it was clear that the light detected by the ICCD was at the ionization front only, with no light emitted from the tail of the discharge. This is to be expected from numerous publications showing fast imaging of guided ionization waves. A similar time-resolved measurement was performed in [9], and in [30] it was shown that the only contribution of the electric field above our detection limit is short-lived and can be associated with the ionization front.

Consequently, when measurements were done without temporal resolution, the detected signal (which covered the length of the entire plume) only showed information concerning the ionization front as it was moving through space, and did not overlay these data with the spectra that could possibly have resulted from a lower electric field in the tail of the discharge.

3.1.2. The increase in the electric field with increasing distance from the capillary. This effect has been previously observed in freely expanding jets in [9, 31], where the slope of the electric field matched the behavior of the velocity profile of the ionization wave. In the present experiment the length of the plume that can be observed with an ICCD (see figure 3) is significantly longer than the length over which the electric field was measured, due to the low intensity of emitted light near the end of the plume. Consequently, the presented profiles do not correspond to the entire visible length of the plume, and the presented results do not suggest that the electric field in the plasma plume only rises.

Figure 3 also shows that the relationship between the length of the visible plume and the gas flow speed is approximately linear for low flow and saturates at flow speeds above 1500 sccm. The electric field profiles on the left-hand side of figure 2 show the same effect—the maximum length at which the electric field is measured is saturated above flow speeds of 1500 sccm. A similar effect was observed in [32].

The cause of the saturation in plume length is discussed in section 3.2.3.

The increase in the electric field in the limited section of the plume is simultaneous with the constriction of the ionization front from an annular shape into a front below 1 mm in diameter [23]. This constriction implies a higher concentration of charge and the resulting electric field, as has already been predicted in numerical simulations [33–36], which we believe to be a probable explanation for the observed effects. The same simulations indicate that the constriction is an effect of gas mixing.

3.1.3. The electric field distribution as a function of gas flow speed. Figure 2 shows that the electric field profile depends on the speed of the gas flow. Even though the nature of the dependence of the electric field on the distance from the capillary remains the same for all flows, it is evident that higher gas flows cause stretching of the electric field profile in space.

Comparing the speed of the gas with other relevant timescales in this discharge, such as the development time of the guided ionization front or the voltage period, it becomes apparent that the speed of the gas flow is sufficiently low to approximate to zero when considering processes in the discharge. However, flow is necessary for the operation of the jet. One possible reason for the need for gas flow is that the flow ensures an atmosphere in the capillary in which breakdown requires a lower voltage, and as such allows for discharge formation when under the same conditions but without the flow a discharge could not form. The same principle would then govern the length of the plume outside the capillary.

Using the same arguments, a significant way in which gas flow can influence a discharge is that it determines the gas mixing in the effluent of the jet [36, 37], and thus the effective ionization and attachment coefficients in the effluent. As those parameters are sensitive functions of gas type, changes in gas mixing are expected to affect charge density and the electric field distribution.

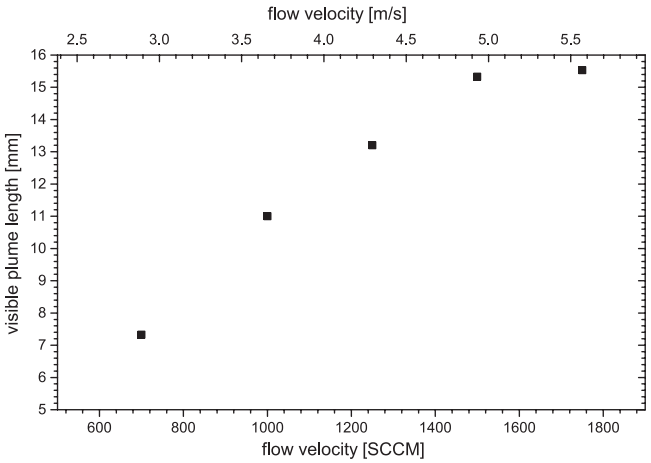

Figure 3. The length of the plume observed by fast imaging. The 4QuikEdig camera was used at the maximum amplification gate at 300 μs and 50 accumulations.

Finally, it has recently been shown [38, 39] that gas composition around the effluent could be one cause for the appearance of guided ionization waves ('plasma bullets') instead of streamers, which are random in space. The essential component around the effluent is the electronegative gas (often oxygen) that forms negative ions around the noble gas effluent. The negative ions then focus the electron avalanche to the center of the noble gas effluent by the means of electrostatics, acting in a way similar to a charged capillary [39].

In the following section the effect of gas mixing on the electric field profile with changing flow is further examined.

3.2. Flow-induced He–air mixing in the effluent of the jet and its effect on the ionization coefficient

3.2.1. Measurements of gas temperature in the effluent of the plasma jet. In order to accurately calculate the gas composition in the effluent, it is necessary to measure the gas temperature. Measurements were performed using a commercial fiber-optic thermometric probe (OpSens, model OTG-F). The temperature is obtained from the shift of the T-dependent band gap edge of a GaAs crystal. The tip of the optical fiber is only 100 μm in diameter and fully dielectric, minimizing disturbances of the plasma plume. Neither the I–V profile of the discharge nor its appearance was affected by the presence of the probe, which leads us to believe that the gas temperatures measured using this technique represent the gas temperatures of an undisturbed jet. Taking into account very low gas temperatures, this was one of the rare techniques that could be used for these measurements with minimal disturbance of the effluent.

The gas temperature profiles as a function of gas flow are given in figure 4. The error bars represent the standard deviation of the measured temperature for 30 s of acquisition with

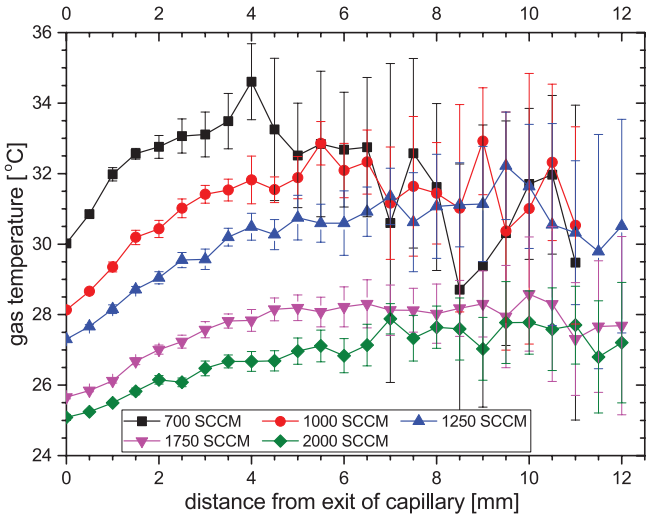

Figure 4. Axial temperature profile in the effluent of the jet.

the highest time resolution of the probe (1 ms) at a given position. The error bars increase drastically with distance from the capillary, where the critical distance is further away from the capillary for higher flows. Coupled with the fact that the visible plume length also increases with increasing flow in this flow range, as shown in figure 3, we believe that gas mixing is responsible for the sudden increase in error bars.

The highest temperatures were recorded for the lowest gas flow and the maximum recorded temperature was 35 °C. The relative change between the gas temperatures at the exit of the capillary and the maximum are less than or equal to 5 °C. Thus, for calculating the gas composition in the effluent of the jet, the difference in the temperature of He and air was not taken into account.

3.2.2. Gas composition in the effluent of the jet and its relationship with the electric field profiles. Figure 5 shows the simulated gas composition in the effluent of the plasma jet. The gas composition and velocity were obtained from a numerical model which solves the Navier–Stokes equation for the He–air mixture together with the diffusion equation for He describing the mixing of the two components. The details of the model can be found in [40], where it was applied to an Ar–H_2 microwave plasma torch and indirectly verified by Rayleigh scattering, and in [41], where it was applied to an atmospheric-pressure Ar radiofrequency-driven atmospheric pressure plasma jet in air and validated with laser-induced fluorescence. To make this model applicable for He–air mixtures the Ar transport and diffusion coefficients had to be replaced with those for He (obtained from [42, 43]) and the buoyant force term, $\mathbf{f} = (\rho_{\mathrm{mix}} - \rho_{\mathrm{air}})\mathbf{g}$, was added to the momentum Navier–Stokes equation. The model does not include heat transfer and assumes the gas mixture to be under ambient conditions. We estimate that neglecting the gas temperature increase of 20 °C causes an error of less than 3% in the calculated velocities and mole fraction, and the main source of uncertainty remains the diffusion coefficients (error due to Chapman–Enskog theory is estimated to be 8% [43]).

The initial mole fraction of air in He already present in the gas flow was taken to be 0.1% molar fraction to reflect the upper bound impurity level in the He flow—the reason for this is found in numerous works showing the importance of impurities for plasma properties such as the density of excited species along the plasma plume or the speed of ionization fronts [38, 44–48]. In [44] it was shown that back-diffusion of air into the jet system (the capillary in our case) can cause as much as 120 ppm of air in He for He flow of 1000 SCCM at a comparable cross section of the plasma channel (the capillary in our case). When the jet was operated in open air without special attention being paid to the gas line, the level of impurities increased to 500 ppm of air for 1000 SCCM flow [44]. The 1000 ppm assumed in this simulation is quite large; however, the calculations were limited to fluid mechanics, excluding all processes that are sensitive to small additions of electronegative species. As will be shown next, the critical levels of air admixture to He in this study were at least an order of magnitude larger than the 1000 ppm of assumed initial air impurities.

Figure 6 shows the evolution of the molar fraction of air as a function of flow at the symmetry axis of the jet, gathered from results shown in figure 5. Two types of characteristic lengths in this jet are added in the same graph: the visible length of the plume as shown in figure 3 and the position at which the maximum E field was measured, taken from data shown in figure 2. For now the discussion will be limited to flows up to 1500 sccm, where the length of the plume increases with the increasing flow at a steady rate, as shown in figure 3.

Correlating the gas composition obtained from the model with the length of the jet (figure 6) reveals that for flow rates up to 1500 sccm the visible plume terminates once the mole fraction of air reaches a value of $x_{\mathrm{Air}} = 0.027 \pm 0.01$, which corresponds to a mass fraction $\omega_{\mathrm{Air}} = 0.163 \pm 0.02$. The errors represent the uncertainty of the model (about 10%). These calculated limiting mole fractions of air in He are an order of magnitude larger than the initial level of air impurities imposed in the gas mixture.

Along the length where the electric field was measured the molar fraction of air does not exceed 0.014; in fact the maximum electric field for flows up to and including 1500 sccm is measured at 0.014 air molar fraction for all flows. This result strongly indicates that the effect of the flow on both the length of the plume and the electric field profile in the plume is governed in large part by gas mixing in this type of jet.

Figure 7 shows the effective Townsend ionization coefficient as a function of the He fraction in a He–air mixture. This represents a case without water in the air; it includes electron attachment to oxygen molecules but does not take into account cross-species ionization (ionization is performed solely by electron impact). Correlating the gas composition from the simulations that correspond to the highest measured electric fields (between 98% and 99% molar fraction of He in electric fields between 16.8×10^5 V m^{-1} and 17.7×10^5 V m^{-1}) it is shown that the effective ionization coefficient is approximately $(1.9 \pm 0.1) \times 10^4$ m^{-1}, where the given interval gives the interval of calculated $\alpha - \eta$.

The idea that a small fraction of air can make a difference in the propagation of ionization fronts is rather old: we would

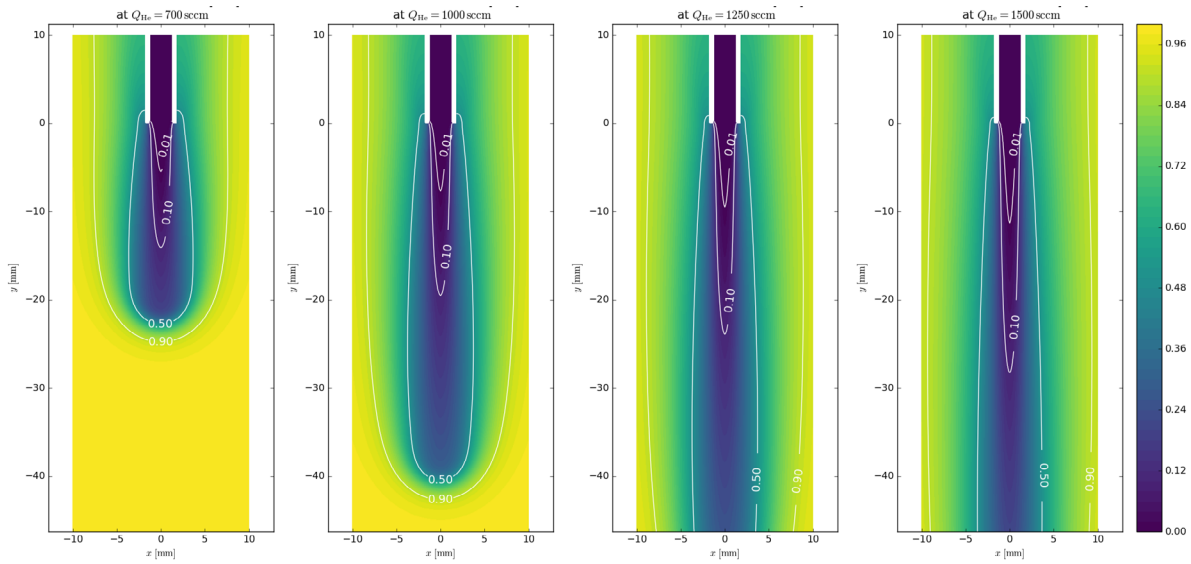

Figure 5. Simulated composition of the effluent of the plasma jet. The scale represents the molar fraction of air in the gas mixture.

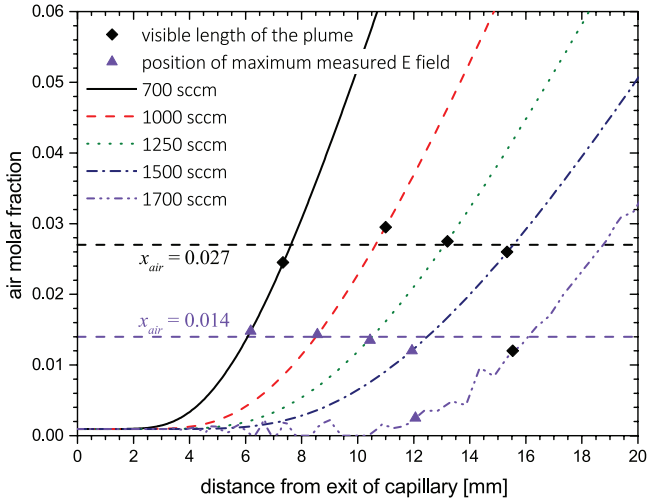

Figure 6. The gas composition close to the jet orifice for various He flow rates. The diamonds indicate the visible length of the plume (from measurements in figure 3), while the triangles show the distance from the capillary where the maximum E field was measured.

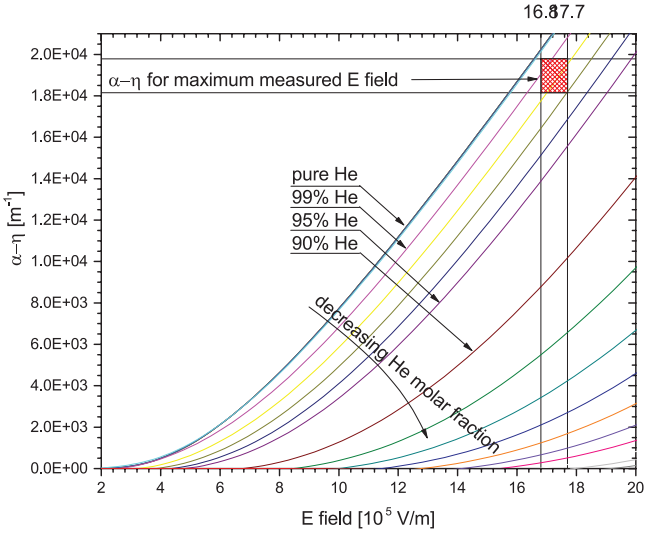

Figure 7. The effective Townsend ionization coefficient (first ionization coefficient, attachment coefficient) for different ratios of He and air. The calculation was performed using Bolsig+ [49] and the LXcat database [50]. The area in the top right corner represents the span of the effective ionization coefficient in this experiment, with an average at 1.9×10^4 m^{-1}, in a 98.5% molar fraction of He.

like to point out work performed on the topic of streamer discharges [51, 52], where it was shown that very small amounts of, for example, oxygen influence streamer development. Following early work on streamers, the effect of impurities on the appearance, length, velocity and chemical content of plasma jets has been reported [44–48].

Recent work [38, 39] has shown the importance of oxygen admixture in the atmosphere into which the plasma plume is expelled. The presence of oxygen has been shown to enable the production of He in its metastable state (He∗) in the plasma plume; this might be partly responsible for the *memory effect* that causes the discharges to propagate along a predetermined trajectory. The abundance and the lifetime of He∗ have been shown to be a function of gas flow [44], and both abundance and lifetime were smaller for lower flows. This effect could be considered to play a role in this work as well; however, the lifetime of He∗ was assessed to be up to 5 μs [38, 39, 44], which is too short to play a role in the work presented in this paper due to the operating frequency of 30 kHz (thus 33 μs between subsequent discharges).

Another role of oxygen in the surrounding atmosphere is to form negative ions and cause the discharge to focus into the previous trajectory [39] giving a *memory effect*, similar to charging the inner walls of the glass capillary. This is considered to be an important factor in the formation of guided ionization waves in place of streamers, which are not reproducible. The experiments in [39] were performed at 940 kHz, and the time between subsequent discharges was short compared with the conditions in this experiment.

The presence of negative ions, however, is not necessary for the existence of discharges, just their transition into *guided* discharges. Beyond this role, the presence of electronegative

gasses in the volume where a discharge is forming is detrimental to discharge development due to their positive electron affinity.

3.2.3. High flows. The visible length of the plume saturates at 1750 sccm. Two main possibilities are considered to explain this: (i) the limited amount of power transferred into the plasma (less that 1 W [22]) and (ii) the possible onset of vortices.

The initial saturation of the visible length of the discharge beyond 1500 sccm could very well be due to the fact that the jet is AC driven and consequently significantly less power is transferred to the plasma compared with pulse-driven jets. This is supported by the literature, where it has been suggested that pulsed plasma kHz-driven jets on average have an order of magnitude higher electron density and electric field and exhibit an order of magnitude higher ionization front velocity [6, 9, 10, 20, 53–57].

Another possible reason is the onset of vortices in the effluent at this high flow rate. The Reynolds number characterizing the flows used in this study is relatively low (143 at a flow of 2000 sccm). Still, the literature has examples where vortices are plasma induced even at low Reynolds numbers [58–65].

Our own measurement using a Schlieren setup (presented in figure 8) shows the onset of vortices at 2000 sccm in the volume where the plasma plume is still visible. The measurement setup consisted of a simple two-lens Schlieren system as described in [66] with a high-power LED at 505 nm as a light source and two lenses of focal length 45 cm . The images were taken with a blade positioned vertically at the focal point of the second lens and recorded with a Princeton PiMAX ICCD camera. The exposure time for every image was 33 μs, or one voltage period.

The top row in figure 8 shows the flow imaged without and with the plasma, with a reference photograph of the visible plasma plume, where it is clear that the visible length of the plasma plume is limited by the vortices induced by the plasma. The bottom row shows that this effect is not present in every voltage period. The three lower images were taken at random during one measurement cycle, at exactly the same flow, under the same laboratory conditions and using the same voltage signal. The vortices were observed at random in the first 2.5 cm outside the capillary. This shows that, in a long measurement for the determination of the plume length or electric field, vortices appeared irregularly but still clearly influenced the visible length and the electric field profile in the plasma plume.

Vortices are of importance because they dramatically enhance the gas mixing, and any further increase in the flow rate does not have an influence on the gas composition, as observed in [41] in Ar and [37]. In [37], the authors observed that the jet terminates at a mass fraction of about 0.5, which is approximately three times higher than in the current work (note that the original work lists a mole fraction of 0.5 but private communications with the authors revealed that the plotted quantity in [37] is, in fact, mass fraction), meaning that the distance that the plume can reach not only depends

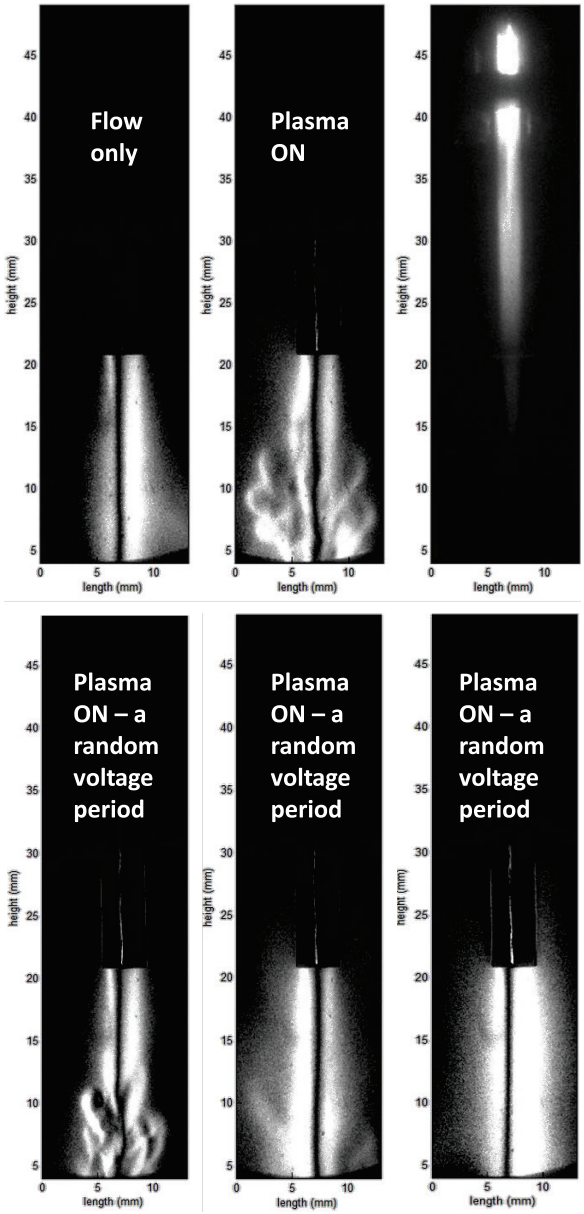

Figure 8. The effluent of the jet obtained by Schlieren imaging in a flow of 2000 sccm. The top row shows the flow without and with the plasma, with a reference image of the visible plume and plasma in the capillary. The bottom row shows three images of the flow taken for three different voltage periods at exactly the same settings and in the same measurement run.

on the gas composition but also on the plasma ignition mechanism. It is reasonable to assume that in the jet described in [37] powered by a pulsed DC power source the maximum power density inside the tube will be higher compared than the AC kHz power source and the plume is, therefore, able to propagate further.

4. Comparison of electric field measurements with previously published data

Previously published data on electric fields associated with plasma bullets are scarce, and available through just a few experimental techniques. The technique used in this work has found

electric field values for AC-driven jets that correspond very well to the values reported on in [5, 9]. A pulsed jet, although in a different geometry, but with a comparable maximum voltage showed the same range of values as the electric field [8]. Finally, in [11], electric field was measured in the vicinity of the capillary in which plasma bullets were propagating. The conditions of flow and gas composition were comparable, the discharge was driven by unipolar pulses of amplitude 15 kV, and as such created very different conditions for discharge development with significantly more power deposited into the plasma. Furthermore, the experiment concerned the discharge in the capillary and the field was measured by a probe 5 mm away from the propagation axis of the plasma. The obtained maximum values were at roughly 5 kV cm^{-1}, which is understandable given the distance from the propagation trajectory.

This work, however, is the first to obtain data on the effect of gas flow on the electric field distribution over the length of the plasma plume in an AC-driven kHz He plasma jet.

5. Conclusions

This paper reports measurements of electric field in a freely expanding 30 kHz AC-driven He jet operated vertically as a function of gas flow speed. The conclusions can be summarized as follows:

(i) While the minimum and the maximum measured electric fields remain unchanged, the effect of the gas flow speed is the stretching of the measured profile in space—the higher the flow, the longer and less steep the electric field profile.

(ii) The electric field was measured along the symmetry axis of the plasma jet and results were obtained along a length shorter than the length of the plume that can be observed by imaging. This portion of the profile showed an increase in the electric field with increasing distance from the capillary, as already reported in [9, 31]. The probable cause for this is the contraction of the plasma bullet as it travels through space away from the capillary, as already reported in many publications.

(iii) There are strong indications that the stretching of the electric field profile with increasing flow speed is caused by differences in gas mixing as a function of gas flow speed. The simulated gas composition shows that the amount of air entrained into the gas flow behaves similarly to the observed behavior of the electric field; in addition we have shown that the visible length of the plasma plume is associated with a 0.027 molar fraction of air in the He flow, while the maximum electric field measured was associated with a 0.014 molar fraction of air and an effective ionization coefficient of 1.9×10^4 m^{-1} (without assumed water impurities).

Acknowledgments

AS would like to thank the European Cooperation in Science and Technology Action COST TD1208 for financial support for a short-term scientific mission. GS, IK, VK, BO and MK would like to thank the Ministry of Education and Science of the Republic of Serbia for financial support through Project 171034 and Project 33022. AO is a Brno PhD Talent Scholarship holder funded by Brno city municipality. The research of LZ was carried out under the project CEITEC 2020 (LQ1601) with financial support from the Ministry of Education, Youth and Sports of the Czech Republic under the National Sustainability Programme II.

References

[1] Iza F, Kim G J, Lee S M, Lee J K, Walsh J L, Zhang Y T and Kong M G 2008 *Plasma Process. Polym.* **5** 322–44
[2] Becker K H, Kersten H, Hopwood J and Lopez J L 2010 *Eur. Phys. J.* D **60** 437–9
[3] Bárdos L and Baránková H 2010 *Thin Solid Films* **518** 6705–13
[4] von Woedtke T, Reuter S, Masur K and Weltmann K D 2013 *Phys. Rep.* **530** 291–320
[5] Sretenovic G B, Krstic I B, Kovacevic V V, Obradovic B M and Kuraica M M 2011 *Appl. Phys. Lett.* **99** 161502
[6] Sobota A, Guaitella O and Garcia-Caurel E 2013 *J. Phys. D: Appl. Phys.* **46** 372001
[7] Keller S, Bibinov N, Neugebauer A and Awakowicz P 2013 *J. Phys. D: Appl. Phys.* **46** 025402
[8] Olszewski P, Wagenaars E, McKay K, Bradley J W and Walsh J L 2014 *Plasma Sources Sci. Technol.* **23** 015010
[9] Sretenović G B, Krstić I B, Kovačević V V, Obradović B M and Kuraica M M 2014 *J. Phys. D: Appl. Phys.* **47** 102001
[10] Wild R, Gerling T, Bussiahn R, Weltmann K D and Stollenwerk L 2014 *J. Phys. D: Appl. Phys.* **47** 042001
[11] Robert E, Darny T, Dozias S, Iseni S and Pouvesle J M 2015 *Phys. Plasmas* **22** 122007
[12] Schoenbach K, Peterkin F, Alden R and Beebe S 1997 *IEEE Trans. Plasma Sci.* **25** 284–92
[13] Tiede R, Hirschberg J, Daeschlein G, von Woedtke T, Vioel W and Emmert S 2014 *Contrib. Plasma Phys.* **54** 118–30
[14] Moisan M, Levif P, Séguin J and Barbeau J 2014 *J. Phys. D: Appl. Phys.* **47** 285404
[15] Isbary G, Zimmermann J, Shimizu T, Li Y F, Morfill G, Thomas H, Steffes B, Heinlin J, Karrer S and Stolz W 2013 *Clin. Plasma Med.* **1** 19–23
[16] Barekzi N and Laroussi M 2013 *Plasma Process. Polym.* **10** 1039–50
[17] Raizer Y P 1991 *Gas Discharge Physics* (Berlin: Springer)
[18] Karakas E and Laroussi M 2010 *J. Appl. Phys.* **108** 063305
[19] Laroussi M, Hynes W, Akan T, Lu X and Tendero C 2008 *IEEE Trans. Plasma Sci.* **36** 1298–9
[20] Xian Y, Lu X, Cao Y, Yang P, Xiong Q, Jiang Z and Pan Y 2009 *IEEE Trans. Plasma Sci.* **37** 2068–73
[21] Boeuf J P, Yang L L and Pitchford L C 2013 *J. Phys. D: Appl. Phys.* **46** 13pp
[22] Sobota A, Guaitella O and Rousseau A 2014 *Plasma Sources Sci. Technol.* **23** 025016
[23] Guaitella O and Sobota A 2015 *J. Phys. D: Appl. Phys.* **48** 255202
[24] Lacoste D A, Bourdon A, Kuribara K, Urabe K, Stauss S and Terashima K 2014 *Plasma Sources Sci. Technol.* **23** 062006
[25] Kuraica M M and Konjević N 1997 *Appl. Phys. Lett.* **70** 1521–3
[26] Kuraica M, Konjević N and Videnović I 1997 *Spectrochim. Acta* B **52** 745–53
[27] Obradovic B M, Ivkovic S S and Kuraica M M 2008 *Appl. Phys. Lett.* **92** 191501
[28] Foster J S 1927 *Proc. R. Soc.* A **117** 137–63

[29] Cvetanović N, Martinović M M, Obradović B M and Kuraica M M 2015 *J. Phys. D: Appl. Phys.* **48** 205201
[30] Darny T, Robert E, Pechereau F, Dozias S, Bourdon A and Pouvesle J 2015 2D time-resolved measurement and modeling of electric fields associated with atmospheric pressure plasma streams propagation in dielectric capillaries *22nd ISPC* pp 1–4
[31] Begum A, Laroussi M and Pervez M R 2013 *AIP Adv.* **3** 062117
[32] Mericam-Bourdet N, Laroussi M, Begum A and Karakas E 2009 *J. Phys. D: Appl. Phys.* **42** 055207
[33] Naidis G V 2010 *J. Phys. D: Appl. Phys.* **43** 402001
[34] Naidis G V 2011 *Appl. Phys. Lett.* **98** 2009–12
[35] Naidis G V 2012 *J. Appl. Phys.* **112**
[36] Lu X, Naidis G V, Laroussi M and Ostrikov K 2014 *Phys. Rep.* **540** 123–66
[37] Xiong R, Xiong Q, Nikiforov A Y, Vanraes P and Leys C 2012 *J. Appl. Phys.* **112** 033305
[38] Winter J, Sousa J S, Sadeghi N, Schmidt-Bleker A, Reuter S and Puech V 2015 *Plasma Sources Sci. Technol.* **24** 025015
[39] Schmidt-Bleker A, Norberg S A, Winter J, Johnsen E, Reuter S, Weltmann K D and Kushner M J 2015 *Plasma Sources Sci. Technol.* **24** 035022
[40] Synek P, Obrusník A, Hübner S, Nijdam S and Zajíčková L 2015 *Plasma Sources Sci. Technol.* **24** 025030
[41] Voráč J, Obrusník A, Procházka V, Dvoák P and Talába M 2014 *Plasma Sources Sci. Technol.* **23** 025011
[42] Lemmon E W, McLinden M O and Friend D G 2016 Thermophysical Properties of Fluid Systems *NIST Chemistry WebBook* (*NIST Standard Reference Database* vol 69) ed P J Linstrom and W G Mallard (Washington, DC: National Institute of Standards and Technology) (http://webbook.nist.gov)
[43] Cussler E L 2009 *Diffusion: Mass Transfer in Fluid Systems* 3rd edn (Cambridge: Cambridge University Press)
[44] Niermann B, Kanitz A, Böke M and Winter J 2011 *J. Phys. D: Appl. Phys.* **44** 325201
[45] Murakami T, Niemi K, Gans T, O'Connell D and Graham W G 2013 *Plasma Sources Sci. Technol.* **22** 15003
[46] Murakami T, Niemi K, Gans T, O'Connell D and Graham W G 2013 *Plasma Sources Sci. Technol.* **22** 045010
[47] Nikiforov A, Li L, Britun N, Snyders R, Vanraes P and Leys C 2014 *Plasma Sources Sci. Technol.* **23** 015015
[48] Winter J, Wende K, Masur K, Iseni S, Dünnbier M, Hammer M U, Tresp H, Weltmann K D and Reuter S 2013 *J. Phys. D: Appl. Phys.* **46** 295401
[49] Hagelaar G J M and Pitchford L C 2005 *Plasma Sources Sci. Technol.* **14** 722–33
[50] LXcat database www.lxcat.laplace.univ-tlse.fr
[51] Ono R and Oda T 2003 *J. Phys. D: Appl. Phys.* **36** 1952–8
[52] Aleksandrov N L, Bazelyan E M and Novitskii G A 2001 *J. Phys. D: Appl. Phys.* **34** 1374–8
[53] Lu X and Laroussi M 2006 *J. Appl. Phys.* **100** 063302
[54] Teschke M, Kedzierski J, Finantu-Dinu E, Korzec D and Engemann J 2005 *IEEE Trans. Plasma Sci.* **33** 310–1
[55] Maletić D, Puač N, Selaković N, Lazović S, Malović G, Dordević A and Petrović Z L 2015 *Plasma Sources Sci. Technol.* **24** 025006
[56] Gerling T, Nastuta A V, Bussiahn R, Kindel E and Weltmann K D K D 2012 *Plasma Sources Sci. Technol.* **21** 034012
[57] Hübner S, Sousa J S, Puech V, Kroesen G M W and Sadeghi N 2014 *J. Phys. D: Appl. Phys.* **47** 432001
[58] Pei X, Ghasemi M, Xu H, Hasnain Q, Wu S, Tu Y and Lu X 2016 *Plasma Sources Sci. Technol.* **25** 035013
[59] Yamada H *et al* 2016 *Japan. J. Appl. Phys.* **55** 01AB08
[60] Zheng Y, Wang L, Ning W and Jia S 2016 *J. Appl. Phys.* **119** 123301
[61] Zhang S, Sobota A, van Veldhuizen E M and Bruggeman P J 2015 *J. Phys. D: Appl. Phys.* **48** 015203
[62] Bradley J W, Oh J S, Olabanji O T, Hale C, Mariani R and Kontis K 2011 *IEEE Trans. Plasma Sci.* **39** 2312–3
[63] Oh J, Olabanji O T, Hale C, Mariani R, Kontis K and Bradley J W 2011 *J. Phys. D: Appl. Phys.* **44** 155206
[64] Foletto M, Puech V, Fontane J, Joly L and Pitchford L C 2014 *IEEE Trans. Plasma Sci.* **42** 2436–7
[65] Boselli M, Colombo V, Ghedini E, Gherardi M, Laurita R, Liguori A, Sanibondi P and Stancampiano A 2014 *Plasma Chem. Plasma Process.* **34** 853–69
[66] Settles G S 2012 *Schlieren and Shadowgraph Techniques: Visualizing Phenomena in Transparent Media* (Berlin: Springer)